ARTICLES
PUBLISHED ONLINE: 19 OCTOBER 2014 | DOI: 10.1038/NNANO.2014.235
nature nanotechnology

Long-range magnetic coupling between nanoscale organic–metal hybrids mediated by a nanoskyrmion lattice

Jens Brede[1]*, Nicolae Atodiresei[2]*, Vasile Caciuc[2], Maciej Bazarnik[3,4], Ali Al-Zubi[2], Stefan Blügel[2] and Roland Wiesendanger[1]

The design of nanoscale organic–metal hybrids with tunable magnetic properties as well as the realization of controlled magnetic coupling between them open gateways for novel molecular spintronic devices. Progress in this direction requires a combination of a clever choice of organic and thin-film materials, advanced magnetic characterization techniques with a spatial resolution down to the atomic length scale, and a thorough understanding of magnetic properties based on first-principles calculations. Here, we make use of carbon-based systems of various nanoscale size, such as single coronene molecules and islands of graphene, deposited on a skyrmion lattice of a single atomic layer of iron on an iridium substrate, in order to tune the magnetic characteristics (for example, magnetic moments, magnetic anisotropies and coercive field strengths) of the organic–metal hybrids. Moreover, we demonstrate long-range magnetic coupling between individual organic–metal hybrids via the chiral magnetic skyrmion lattice, thereby offering viable routes towards spin information transmission between magnetically stable states in nanoscale dimensions.

Recent experimental and theoretical advances[1–12] in the understanding of spin injection from ferromagnets into organic molecules have led to increased efforts towards tailoring organic–metal interfaces for specific applications in molecular spintronics[13,14]. On the one hand, several methods have been proposed theoretically to tune the magnetic properties of organic–metal hybrids by means of chemical functionalization[8,10,15]. On the other hand, spin-resolved microscopic and spectroscopic techniques, such as spin-polarized scanning tunnelling microscopy (SP-STM) and spectroscopy, have helped greatly in revealing spin-dependent phenomena at organic/ferromagnet interfaces with a spatial resolution down to the atomic scale[3,6,8,16,17]. In parallel with advances in the field of molecular-based spintronics, rapid progress has been made in understanding atomic spin systems on surfaces[18–22]. In particular, the magnetic anisotropies of single atoms have been determined and subsequently controlled via the local environment. Moreover, electronic decoupling of single atoms from substrate electrons with thin insulating layers[20] has been shown to drastically increase the lifetimes of magnetic states. The bottom-up fabrication of few-atom clusters by STM manipulation has been demonstrated to yield essentially stable magnetic bits at cryogenic temperatures[22,23] or functional atomic-scale spin-logic devices[18] when antiferromagnetic spin chains are coupled to magnetically stable input gates.

Here, we fabricate organic–metal hybrids with tunable lateral dimensions on the nanoscale by depositing sp^2-conjugated organic carbon systems, that is, single coronene (Cor) molecules or graphene (Gr) islands, on a magnetic skyrmion lattice (SkX) of a single atomic layer of Fe on an Ir(111) substrate[24]. Although the SkX does not exhibit a net magnetic moment and thus does not align with an external magnetic field[24], the strong interaction between the Fe atoms and the organic material leads to the formation of local organic–ferromagnetic (organic–FM) units that can be switched by an external field. Controlling the lateral dimensions of the organic carbon systems enables tuning of the experimentally determined switching fields of the nanoscale organic–metal hybrids by SP-STM. State-of-the-art first-principles calculations elucidate how the exchange coupling, magnetic moment, as well as magnetocrystalline anisotropy energy can be controlled on the atomic scale, with magnetic moments from a few tens up to several thousands of Bohr magnetons (μ_B) and magnetocrystalline anisotropy energies of few millielectronvolts (meV) up to several eV. When the magnetocrystalline anisotropy energy is tailored to match the exchange coupling of the nanoscale organic–metal hybrid to its surroundings, we find a correlated magnetization reversal behaviour of individual organic–metal hybrids, indicating long-range magnetic coupling mediated by the chiral nanoskyrmion lattice, thereby opening up new avenues to control, couple and manipulate the spin properties of metal–organic hybrid systems at the nanoscale.

Organic–FM units in a skyrmion lattice under magnetic field

In a first step we studied organic–FM units consisting of Cor molecules on the Fe monolayer on Ir by SP-STM. All measurements were performed at a temperature of 6.5 K and in ultrahigh vacuum (UHV). A representative overview image is shown in Fig. 1a. The bare Fe monolayer exhibits a square lattice with a periodicity of ~1 nm. This chequerboard pattern is characteristic for the SkX imaged with an out-of-plane magnetized SP-STM probe tip[24]. The experimentally deduced (Supplementary Section I) adsorption geometry of the Cor molecules is presented in the inset of Fig. 1a. We will refer to a Cor molecule together with the

[1]Institute of Applied Physics and Interdisciplinary Nanoscience Center Hamburg, University of Hamburg, D-20355 Hamburg, Germany, [2]Peter Grünberg Institut (PGI-1) and Institute of Advanced Simulation (IAS-1), Forschungszentrum Jülich and JARA, 52428 Jülich, Germany, [3]Institute of Physics, Poznan University of Technology, Piotrowo 3, 60-965 Poznan, Poland, [4]Institute of Applied Physics and Interdisciplinary Nanoscience Center Hamburg, University of Hamburg, D-20355 Hamburg, Germany. *e-mail: jbrede@physnet.uni-hamburg.de; n.atodiresei@fz-juelich.de

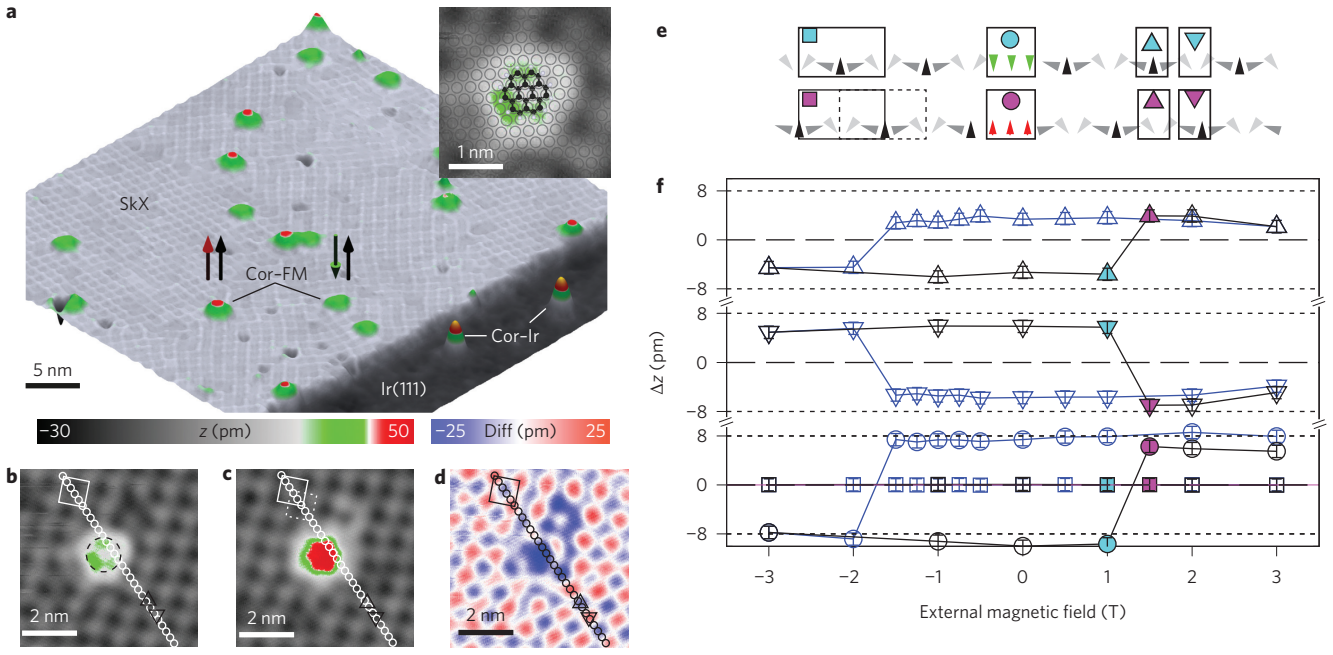

Figure 1 | SP-STM images of Cor–FM units embedded in a SkX under an external magnetic field. a, Pseudo-three-dimensional representation of an SP-STM image of Cor–FM units in an Fe monolayer on Ir: square lattice of the SkX in light grey; Ir(111) substrate in dark grey; Cor–FM units (green, green-red) and Cor on Ir(111) (Cor-Ir) in green-red-yellow. The magnetization directions of two representative Cor–FM units with respect to the magnetization direction of the tip (black arrows) are indicated by green and red arrows, respectively. Inset: Experimentally deduced Cor–FM unit adsorption geometry (Supplementary Figs 1 and 2), atomic Fe lattice (grey circles) and Cor structure (black), superimposed on a zoom into the SP-STM image given in **b**. **b**,**c**, SP-STM images of a Cor–FM unit in the ↓↑ (**b**, green) and the ↑↑ (**c**, red) states. **d**, Change in magnetization, conveniently visualized in a difference image ('image **d** = image **b** − image **c**'): blue/red areas indicate a switch of magnetization from ↓↑/↑↑ to ↑↑/↓↑. In **b**–**d**, the unit cell (square) and sub-units (upward and downward triangles, respectively) of the SkX and the Cor–FM unit (dashed circle) are indicated. Dashed square in **c**: SkX unit cell shifted by half a period. **e**, Schematic side-view illustration of the magnetization profile (cones depict the local magnetization direction, Supplementary Fig. 3) along the atoms indicated by the row of circles in **b** (top) and **c** (bottom). Black rectangles outline different parts: unit cell (square) and sub-units (triangles) of the SkX as well as the Cor–FM unit (circle). Dashed rectangle: SkX unit cell shifted by half a period. In **e** and **f**, cyan and magenta colours indicate schematics and data corresponding to **b** and **c**, respectively. **f**, Change in height (Δz) of the Cor–FM unit (circles), the SkX unit cell (squares) and the two SkX sub-units (upward and downward triangles, respectively) as deduced from SP-STM images, plotted for various values of external magnetic field. Error bars indicate the noise level in z. The black/blue traces are for subsequently increasing/decreasing fields. The Cor–FM unit and SkX sub-units exhibit a clear hysteresis, while the overall SkX does not. Tunnelling parameters: $V = 50$ mV and $I = 2$ nA (**a**–**c**). The same colour scale is used for the inset in **a**, and in **b** and **c**. External magnetic field applied: 1 T (**a**,**b**) and 1.5 T (**c**).

underlying 12 Fe atoms as a 'Cor–FM unit'. Cor–FM units exhibit a binary (red/green) contrast in SP-STM images. This contrast corresponds to a magnetization direction parallel (↑↑) or antiparallel (↓↑) with respect to the tip magnetization direction, respectively. The response of the sample to an external out-of-plane magnetic field H is evaluated as follows. In Fig. 1b, a typical SP-STM image of a Cor–FM unit at $H = 1$ T is presented and the SkX unit cell as well as two sub-units are indicated by the square and triangles, respectively. By increasing H to 1.5 T and subsequently recording another SP-STM image (Fig. 1c), an increase in the apparent height of the Cor–FM unit and inversion of the contrast of the SkX are clearly visible. The changes in apparent height due to magnetization reversal are conveniently visualized in the difference image in Fig. 1d, where blue/red areas indicate a switching of the magnetization from ↓↑/↑↑ to ↑↑/↓↑. The apparent height changes derived from Fig. 1b,c as a function of the externally applied field yield magnetization curves (Supplementary Section II and Supplementary Movie) such as those presented in Fig. 1f. The black/blue traces correspond to a measurement series with increasing/decreasing field H. The SkX (squares) does not show a net change in magnetization, but the two SkX sub-units (upward and downward triangles) show hysteretic behaviour due to shifting of the SkX by half a unit cell. The shifting correlates with a magnetization reversal of the Cor–FM unit (circles). A schematic side view representation of the changes in local magnetization for the atoms indicated by the circles in Fig. 1b–d are presented in Fig. 1e (Supplementary Section III). The full spatial information of the magnetization-reversal is clearly seen in the difference image in Fig. 1d: (1) uniform contrast at the Cor–FM unit site due to flipping of the Cor–FM unit's magnetization direction and (2) alternating contrast giving rise to a chequerboard pattern for the SkX due to a shift of half a unit cell.

Switching fields of organic–FM units in a skyrmion lattice

In a second step we studied organic–FM units with lateral dimensions of several tens of nm^2. We will refer to these larger units, consisting of graphene islands on the Fe monolayer on Ir, as 'Gr–FM units'. A representative SP-STM overview image of Gr–FM units together with the SkX is presented in Fig. 2a. The Gr–FM units exhibit a characteristic Moiré pattern with a pronounced corrugation of ∼0.15 nm in the STM topography[25]. The SP-STM image reveals again the familiar two-level contrast (red/green) of the different Gr–FM units, corresponding to a magnetization direction parallel or antiprarallel with respect to the tip magnetization direction, respectively. We now evaluate the apparent height of the Gr–FM units as a function of an external out-of-plane magnetic field H. In Fig. 2b, a typical hexagonal Gr–FM unit with an area of ∼65 nm^2, corresponding approximately to 1,000 Fe atoms, is shown with $H = 6$ T applied. On increasing H to 6.5 T and subsequently recording another SP-STM image (Fig. 2c), the increase in apparent height of the Gr–FM unit is striking. The changes in

apparent height due to magnetization reversal are revealed in the difference image in Fig. 2d, where the blue/red areas indicate a switch of the magnetization from ↓↑/↑↑ to ↑↑/↓↑. The Gr–FM unit shows a uniform contrast (blue), while the surrounding SkX exhibits the familiar chequerboard pattern. Note that the Gr–FM unit is situated at the boundary of two rotational SkX domains (the domain boundary is indicated by a dashed line).

The average apparent height of the area indicated by the dashed circle in Fig. 2b is deduced for both SP-STM images (Fig. 2b,c) as a function of the externally applied field, yielding the upper magnetization curve presented in Fig. 2e. For comparison, the magnetization curve of a typical Cor–FM unit is shown in the lower part of Fig. 2e. The black/blue traces correspond to a measurement series with increasing/decreasing field H. From the magnetization curves we deduce a switching field of $H_C^{Gr-FM} \approx 6.25$ T and $H_C^{Cor-FM} \approx 1.25$ T, respectively.

We performed similar measurements for more than 350 organic–FM units, and the distributions of switching fields are given in Fig. 2f for Gr–FM units (top) and Cor–FM units (bottom). The majority of studied Gr–FM units (yellow column) did not switch at ~6.5 T, which was the highest field available in our experimental set-up. Several results are particularly noteworthy: (1) a remarkably high coercivity of large organic–FM units, exceeding that of Gr-covered Co-islands[25]; (2) hysteretic behaviour during magnetization reversal, even for ultra-small Cor–FM units; (3) the large spread of the observed coercive fields for Cor–FM units; and (4) a correlation between organic–FM unit magnetization reversals and a shift of half a unit cell in the surrounding SkX. Points (3) and (4) can be explained by interaction effects, but first we elucidate the origin of the remarkable stability of the organic–FM units and turn to first-principles density functional theory (DFT) calculations.

Magnetic properties of organic–FM units by DFT

The fully relaxed geometries obtained from DFT for both graphene and Cor on the Fe monolayer on Ir(111) are depicted Fig. 3a,c. First, we compare the relative position of the C atoms with respect to the underlying Fe surface and their resulting magnetic properties for Gr/Fe/Ir(111). The Fe atoms at the top site (in Fig. 3a, semi-transparent spheres interconnected with a red arrow and labelled J_1) are situated beneath the centre of a C_6 ring where the Fe–C distance is ~3.6 Å. Here, the Fe atoms have a magnetic moment of $\mu_1 \approx 2.8\ \mu_B$, an exchange coupling constant of $J_1 \approx 2.3$ meV μ_B^{-2} and a magnetocrystalline anisotropy energy constant of $K_1 \approx 0.6$ meV/Fe atom, very similar to the values for Fe atoms of the pristine Fe/Ir(111) surface. This is in line with previous studies showing that the graphene layer is physisorbed at the top sites and is only very weakly interacting with the surface[25]. The situation is very different for the valley sites. Here, strong hybridization of C and Fe with a bond length of only ~2.0 Å significantly modifies the spin-dependent electronic structure of the Fe atoms. Consequently, the magnetic properties are strongly changed to $\mu_2 \approx 2.1\ \mu_B$, $J_2 \approx 7.5$ meV μ_B^{-2} and $K_2 \approx 0.35$ meV/Fe atom.

It is instructive to follow the evolution of μ, J and K of the Fe atoms as a function of Fe–C distance (Fig. 3b). A monotonous decrease is observed in the magnetic moment of the Fe atoms from their pristine value of $\mu_0 \approx 2.8\ \mu_B$ (indicated by the dashed line) when the Fe–C distance is less than 2.7 Å to a value of $\mu \approx 2.3\ \mu_B$ when the Fe–C distance is ~2.0 Å, which is accompanied by a monotonous increase in the exchange coupling strength between Fe atoms from the pristine value of $J_0 \approx 2$ meV μ_B^{-2} to $J_2 \approx 7$ meV μ_B^{-2}. Both effects are readily understood as a consequence of p–d hybridization[8] as the electronic states of C and Fe atoms start hybridizing according to their spatial extension normal to the surface plane: C p_z orbitals overlap with Fe d_{z^2} states, and newly formed p–d hybrid states increase the spectral

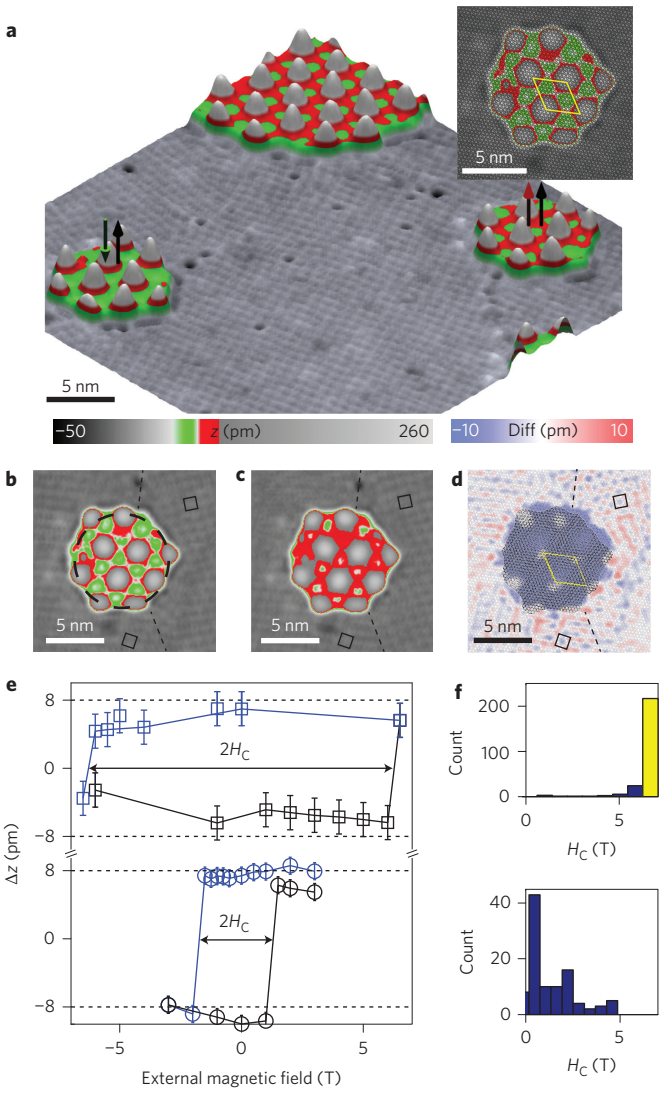

Figure 2 | Magnetic switching fields of organic–FM units embedded in a SkX measured by SP-STM. a, Pseudo-three-dimensional representation of Gr–FM units in a monolayer of Fe on Ir(111): SkX in light grey; Gr–FM units in green-red-grey. The magnetization directions of two representative Gr–FM units with respect to the tip's magnetization direction (black arrows) are indicated by green and red arrows, respectively. Inset: Tentative model of the atomic Fe lattice (grey circles) and the graphene layer (black) superimposed on a zoom into the SP-STM image given in **b**. The unit cell of graphene/Fe/Ir is indicated by the yellow parallelogram. **b**,**c**, SP-STM images of a Gr–FM unit in the ↓↑ (**b**) and the ↑↑ (**c**) states. Squares indicate the unit cell of the SkX and the dashed line marks a domain boundary in the SkX. **d**, Change in magnetization, conveniently visualized in a difference image: blue/red areas indicate a switch of magnetization from ↓↑/↑↑ to ↑↑/↓↑. The difference image is superimposed with the same tentative model as shown in the inset of **a**. **e**, Change in height (Δz) of the Gr–FM unit (squares) evaluated in the area indicated by the dashed circle in **b**, plotted for various external magnetic fields. The black/blue traces are for subsequently increasing/decreasing fields. For comparison, a magnetization curve of a Cor–FM unit (circles) is provided. Error bars indicate the noise level in z. **f**, Histograms of all measured switching fields (H_C) for Gr–FM units (top) and Cor–FM units (bottom), respectively. The switching fields of Gr–FM units, indicated by the yellow column, exceed 6.5 T, the maximum field available in our set-up. Tunnelling parameters: $V = 75$ mV and $I = 0.5$ nA (**a**–**c**). The same saturated colour scale was used in the inset of **a**, and in **b** and **c**. External magnetic field applied: –1 T (**a**), 6 T (**b**) and 6.5 T (**c**).

weight of the hybrid at the Fermi level, thereby increasing the exchange coupling J of neighbouring Fe atoms, while simultaneously decreasing the overall magnetic moment as the newly formed hybrid states below the Fermi energy are situated predominantly in the minority channel[8]. (For the spin-polarized projected density of states of the Cor–FM unit as well as a detailed list of all determined parameters, see Supplementary Section VI.) The evolution of K with decreasing Fe–C distance shows a peculiar behaviour: a substantial increase from ~0.6 to ~0.9 meV/Fe atom when the Fe–C distance is reduced from ~3.3 to ~2.65 Å, after which it decreases to a value of ~0.3 meV/Fe atom at a distance of 2 Å. This trend of increasing K at large distances is particularly noteworthy, as the hybridization in Fe–C is very small. This is reflected in the negligible change in both J and μ at these Fe–C distances, opening a novel route towards tailoring the magnetocrystalline anisotropy energy at large Fe–C distances.

Next, we turn to the Fe atoms beneath the Cor molecule (Fig. 3c). Their adsorption geometry, magnetic moment and exchange coupling are very similar to those for Fe atoms at valley sites for Gr/Fe/Ir (111). The C atoms are directly on top of Fe atoms, the Fe–C bond length is ~2.0 Å, the magnetic moment is $\mu_3 \approx 2.1\ \mu_B$ and the exchange coupling is $J_3 \approx 9.9$ meV μ_B^{-2}. Interestingly, the magnetocrystalline anisotropy energy constant is significantly increased to $K_3 \approx 2.6$ meV/Fe atom. Qualitatively, this increase in K is readily understood as a consequence of the reduced dimensionality of a magnetic particle, where polarization, coordination and edge effects become increasingly important[19]. Moreover, we see a drastic difference for the Fe-edge atoms beneath the Cor molecule: the bond length and magnetic moment are similar to those of the central atoms, but the exchange coupling towards the outside is greatly reduced to $J_4 \approx 1.2$ meV μ_B^{-2}, which is less than half the value of the bare Fe surface.

Two main effects can be derived from our DFT calculations: (1) magnetic hardening[15,25] facilitates a very robust ferromagnetic coupling of the Fe atoms within organic–FM units, resulting in nanomagnets with a total magnetic moment M_T approximated by the number N of Fe atoms times the atomic magnetic moment ($M_T = N{\cdot}\mu$) and a total magnetocrystalline anisotropy energy given by $\Delta E = N{\cdot}K$, and (2) magnetic softening eases a switching of the nanomagnets with respect to the surrounding Fe layer[26]. Note that for a typical Gr–FM unit (Fig. 2b) this implies $M_T^{Gr-FM} \approx 2{,}000\mu_B$ and $\Delta E^{GR-FM} \approx 0.5$ eV, while for a Cor–FM unit (Fig. 1b) $M_T^{Cor-FM} \approx 25\mu_B$ and $\Delta E^{Cor-FM} \approx 30$ meV.

To compare our theoretically deduced values with our experiment we deduced the energy barrier for magnetization reversal from the measured switching fields of the organic–FM units as a function of hybrid size. A detailed analysis following the methodology outlined by Ouazi *et al.*[27] (Supplementary Section VII), shows a linear dependence of the magnetocrystalline anisotropy energy on the number of Fe atoms incorporated in organic FM units. In excellent agreement with our first-principles calculations, we deduce a K of 0.3–0.5 meV/Fe atom for Gr–FM units and 1.3–2 meV/Fe atom for Cor–FM units. In particular, we note a trend towards higher values of K for smaller organic–FM units due to the reduced dimensionality[19].

Furthermore, we note another prediction of our calculations: if we define an effective coupling constant J_{eff} of the Cor–FM unit towards the surroundings, we obtain a value of $[(6\times3)+(3\times2)]\times J_4 \approx 29$ meV μ_B^{-2}, which is comparable to its total magnetocrystalline anisotropy energy ΔE^{Cor-FM}. In other words, switching the magnetization direction of (all) Fe atoms around the Cor–FM unit is expected to cause a magnetization reversal of the hybrid itself. In reality, we do not have a ferromagnetic Fe layer surrounding our Cor–FM units, but the non-collinear spin-texture of the SkX, which does not have uncompensated magnetic moments. However, we have already demonstrated a correlation of flipping

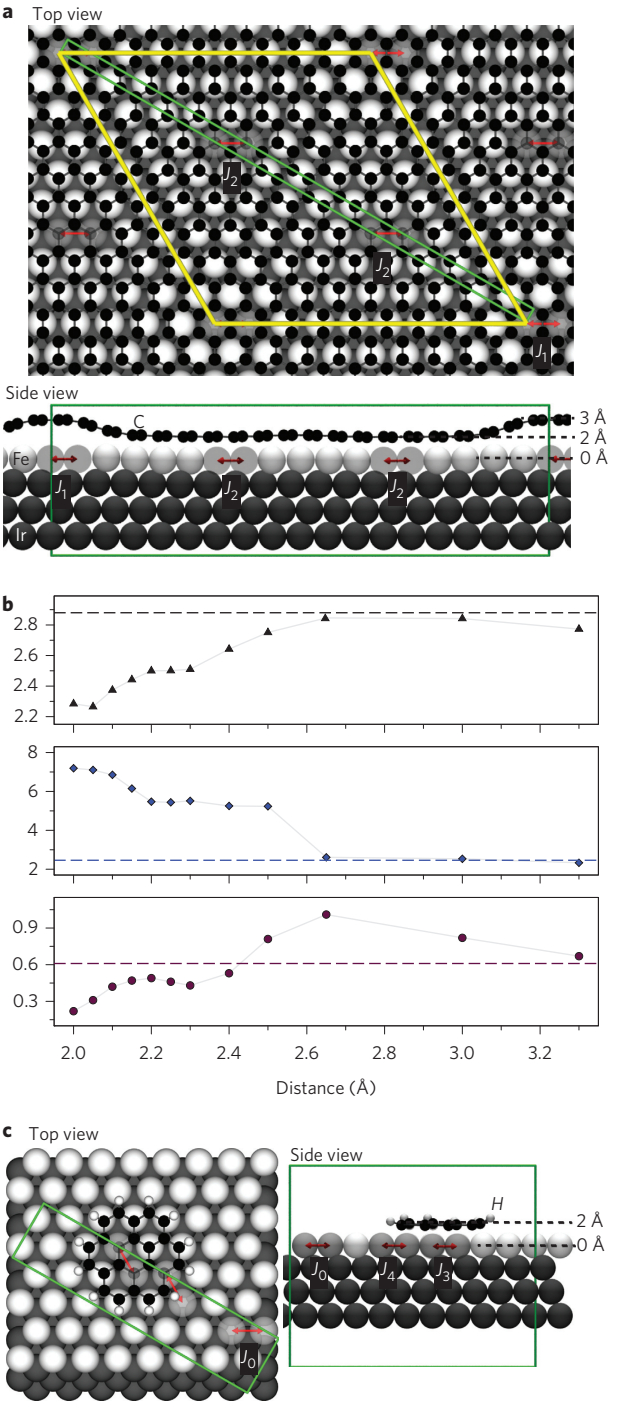

Figure 3 | Adsorption geometry, magnetic moment μ, exchange coupling constant J and magnetic anisotropy energy constant K for graphene and coronene on an Fe monolayer on Ir(111) by DFT. a, Relaxed geometry of graphene (small black spheres) on Fe (light grey spheres) on Ir(111) (dark grey spheres). The unit cell (yellow parallelogram) and coupling constants J_1 and J_2 (red arrows) between Fe atoms at high symmetry sites are indicated. The green rectangle is a guide to the eye: only atoms in the plane of the rectangle are displayed in the side view. **b**, Evolution of μ (upper graph, in units of μ_B), J (middle graph, in units of meV μ_B^{-2}) and K (lower graph, in meV/Fe atom) of Fe atoms as a function of Fe–C distance. Dashed lines indicate pristine values. **c**, Relaxed geometry of Cor (small black white spheres) on Fe (light grey spheres) on Ir(111) (dark grey spheres). The green rectangle is a guide to the eye: only atoms in the plane of the rectangle are displayed in the side view. The values are $J_3 \approx 9.9$ meV μ_B^{-2}, $\mu_3 \approx 2\ \mu_B$, $K_3 \approx 2.6$ meV, $J_4 \approx 1.2$ meV μ_B^{-2}, $\mu_4 \approx 2.2\ \mu_B$ and $K_4 \approx 2.6$ meV.

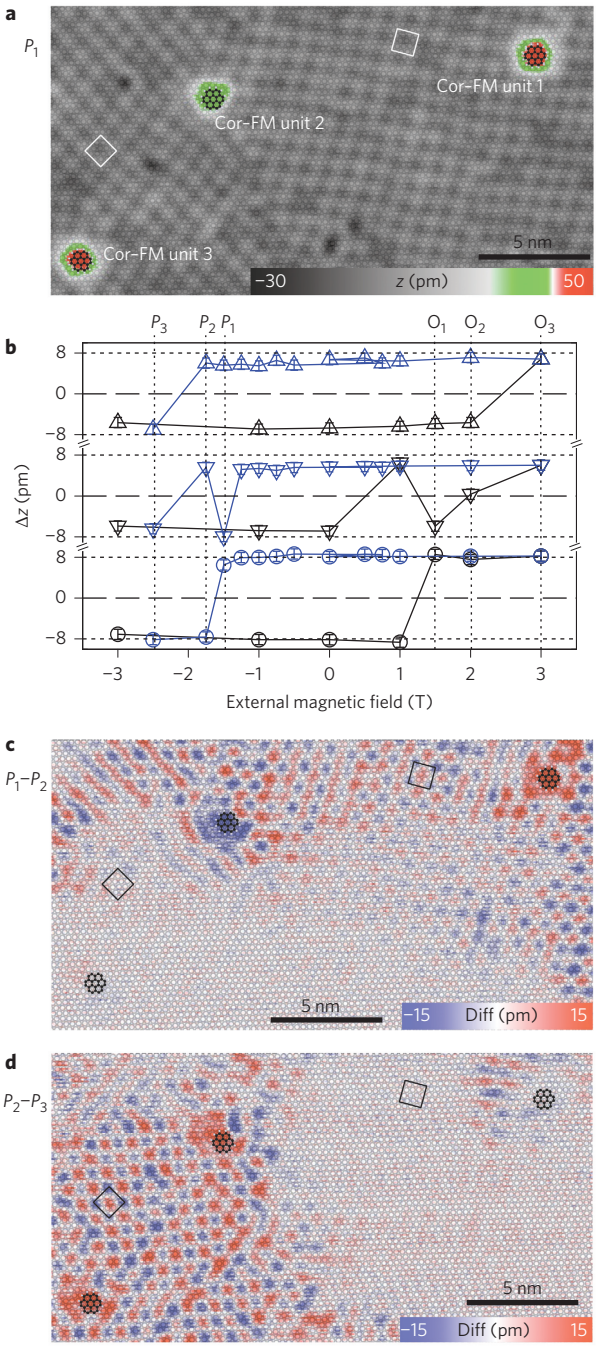

Figure 4 | Magnetic coupling of Cor–FM units via a SkX by SP-STM. **a**, Zoom into an SP-STM image of three Cor–FM units embedded in the SkX, recorded with an applied external magnetic field of –1.5 T. As a guide to the eye, the atomic lattice (grey spheres), Cor structures (black spheres) and two SkX unit cells (white squares) are superimposed. **b**, Magnetization curves for Cor–FM unit 1 (circles), Cor–FM unit 2 (downward triangles) and Cor–FM unit 3 (upward triangles). Error bars indicate the noise level in *z*. **c**,**d**, Difference images for the values of external magnetic field as indicated by P_1 to P_3, illustrating the magnetic coupling of unit 2 to both unit 1 and unit 3 via the non-collinear spin-texture of the SkX. As a guide to the eye, the atomic lattice, Cor structures and SkX unit cells are superimposed onto the images. Tunnelling parameters: $I = 2$ nA, $V = 50$ mV.

the magnetization direction of the Cor–FM unit with a shift of half a unit cell of the surrounding SkX. Because the Cor–FM units couple to the SkX they may in turn couple, even over large distances, via the SkX, enabling information transfer by vector spin chirality[28].

Magnetic coupling of organic–FM units in a skyrmion lattice

We address the coupling via the complex spin-texture of the nano-skyrmion lattice of Fe/Ir(111), by studying an ensemble of three Cor–FM units (Fig. 4a). As a guide to the eye we have overlaid the experimental data with the atomic lattice as well as Cor models. The magnetization curves corresponding to Cor–FM units 1 to 3 are presented in Fig. 4b. When focusing on unit 2, a peculiar behaviour is apparent: at $H = -1.75$ T the hybrid has switched from parallel back to the antiparallel alignment with respect to the external magnetic field. To elucidate the origin of this unusual behaviour we calculated the difference images in Fig. 4c,d. In Fig. 4c, unit 1 has a red contrast as a result of aligning parallel with the external field, and the familiar chequerboard contrast extends away from the molecule all the way to unit 2, which has a blue contrast as a consequence of aligning antiparallel to the applied *H*. From this observation we can derive two conclusions: (1) the change induced in the spin-texture of the SkX due to switching of a Cor–FM unit is highly non-local and extends over several nanometres, and (2) the effective coupling strength of the SkX to Cor–FM unit 2 is sufficient to trigger a magnetization reversal of unit 2 to the energetically less favourable configuration antiparallel to the applied external magnetic field. The observed magnetic contrast in the difference images can be understood within the vector spin chirality model previously used to explain the magnetic contrast for one-dimensional finite atomic chains[28]: upon switching the magnetization of unit 1, the entire spin-texture of the SkX shifts by half a unit cell and the information is transmitted to unit 2, which likewise flips due to exchange coupling to the chiral SkX. When decreasing *H* further to –2.5 T, unit 3 aligns parallel with the field, as well as unit 2. The spin-texture connecting the two again shows profound contrast in the corresponding difference image (Fig. 4d). Interestingly, the non-trivial magnetization reversal occurs again when reversing the magnetization loop (black trace in Fig. 4b, in particular points O_1–O_3). The coupling is robust and reproducible. About 10% of all studied Cor–FM units switched from the parallel back to the energetically less favourable antiparallel configuration during the aquisition of magnetization curves (Supplementary Section VIII shows further examples). The fact that not all Cor–FM units switched back is understood to be a consequence of the complex spin-structure at the Cor–FM–SkX interface (Supplementary Section III). The coupling of the three-fold symmetric Cor–FM unit into the four-fold symmetric SkX (with its three rotational domains) as well as the inherent flexibility of the SkX due to its incommensurability with the underlying atomic lattice[24], facilitates highly non-collinear spin-textures at the interface. These are, in a first approximation, characterized by differences in the effective coupling constant as well as the effective anisotropy energy of a particular Cor–FM unit, thereby explaining the large spread of observed switching fields as discussed above. This is in line with the absence of switching back to an antiparallel configurations for the larger Gr–FM units: their anisotropy energy is too large to be overcome by coupling to the SkX. Finally, we note that an inherent maximum of the coherence length of information transfer via the SkX was not observed. The translation of the SkX triggered by the switching of an organic–FM unit propagated until a defect or the next organic–FM unit was reached.

Conclusions

The adsorption of organic molecules directly on (magnetic) metal surfaces leads to drastic modifications of the molecular states due to hybridization, and in turn also modifies the electronic properties of the metallic support, resulting in the formation of novel interface states. While the organic molecules can generally be regarded as a small perturbation to the overall electronic structure of the metallic support in bulk-like systems, their influence on the interface and surface states can be significant and is becoming increasingly important as the dimensions of studied systems are reduced to the

nanoscale. Here, we have shown that organic systems can be used to tailor the magnetization reversal of nanoscale hybrids embedded in a non-collinear spin-texture. We have designed organic–metal hybrids of various lateral sizes with switching fields from a few millitesla up to several tesla and anisotropy barriers ranging from a few meV to a few eV. Magnetic hardening by organic adsorbates[15,25] is used to enable a robust ferromagnetic coupling down to the single-molecule level. Moreover, hybrids consisting of only 12 Fe atoms showed a significant increase in magnetocrystalline anisotropy energy per Fe atom, thereby stabilizing even the ultrasmall hybrids against thermally activated magnetization reversal. Most importantly, we found that we could tune the magnetocrystalline anisotropy energy of hybrids to match the coupling strength to the non-collinear spin state of a nanoskyrmion lattice and demonstrate long-range coupling of individual nanohybrids over a distance of several nanometres mediated by a chiral nanoskyrmion lattice. We anticipate our work to be a starting point for more experimental as well as theoretical efforts toward the realization of functional organic–metal hybrid devices such as spin-logic units, which demonstrate functionality similar to that of single-atom logic gates[18]. By using chemical means to tune the relevant anisotropy barriers, as demonstrated in this work, operational temperatures can be raised substantially compared with previous model systems[22,23].

Methods

All sample preparations and experiments were performed *in vacuo*. The Ir(111) single crystal was prepared using standard procedures: cycles of Ar^+-ion bombardment with successive annealing in an O^2 background pressure of 1×10^{-7} mbar followed by high-temperature heating under UHV conditions ($<1 \times 10^{-9}$ mbar). Sample quality was assured directly by atomic-resolution STM measurements. The ultrathin film of ~1 monolayer (ML) Fe was deposited by means of electron bombardment of an Fe-rod (purity of 99.999%) at a base pressure of $<1 \times 10^{-10}$ mbar and a flux of 0.5 ML min^{-1} in a direct line of sight onto the Ir substrate at temperatures slightly above room temperature. Afterwards, Cor molecules were deposited from a home-built Knudsen cell onto the sample (held at room temperature) at a nominal rate of 3 ML min^{-1} at a background pressure of $<1 \times 10^{-10}$ mbar. Finally, the sample was transferred directly into the STM and cooled to the measurement temperature of 6.5 K. Graphene islands were grown following a procedure described elsewhere[25] and intercalated with Fe by deposting Fe onto the Gr/Ir(111) surface held at 400 K during deposition. Similar results were obtained using thermally induced Cor decomposition directly onto the Fe film (Supplementary Section V). Our SP-STM tips with negligible stray fields were prepared by depositing ~20 ML of Cr *in situ* onto *in vacuo* flashed W tips. Magnetic out-of-plane sensitivity was ascertained *in situ* on the Fe/Ir(111) sample. All SP-STM images were taken in constant-current mode. First-principles DFT calculations were carried out with pseudopotentials generated with the projector augmented wave (PAW) method as implemented in the VASP code[29,30]. We also used the Perdew–Burke–Ernzerhof (PBE) exchange-correlation energy functional, and the Kohn–Sham eigenstates were expanded in a plane wave basis set determined by a cutoff energy of 500 eV. The system Gr/Fe/Ir(111) was modelled by a 10×10 Gr unit cell (200 C atoms) on a 9×9 Fe/Ir(111) unit cell (one layer of Fe and three layers of Ir, that is, 81 Fe atoms and 243 Ir atoms). For the Cor–FM unit—to avoid molecule–molecule interactions due to the periodic boundary conditions—a single Cor on Fe/Ir(111) was modelled by a 22×19 Å rectangular supercell comprising one Fe layer on top of three Ir. Overall, the threshold value for the calculated Hellmann–Feynman forces used to obtain the ground-state molecule–surface adsorption geometry was set to 0.001 eV $Å^{-1}$.

Received 7 May 2014; accepted 13 September 2014; published online 19 October 2014

References

1. Dediu, V., Murgia, M., Matacotta, F. C., Taliani, C. & Barbanera, S. Room temperature spin polarized injection in organic semiconductor. *Solid State Commun.* **122,** 181–184 (2002).
2. Xiong, Z. H., Wu, D., Valy Vardeny, Z. & Shi, J. Giant magnetoresistance in organic spin-valves. *Nature* **427,** 821–824 (2004).
3. Iacovita, C. *et al.* Visualizing the spin of individual cobalt-phthalocyanine molecules. *Phys. Rev. Lett.* **101,** 116602 (2008).
4. Cinchetti, M. *et al.* Determination of spin injection and transport in a ferromagnet/organic semiconductor heterojunction by two-photon photoemission. *Nature Mater.* **8,** 115–119 (2009).
5. Gambardella, P. *et al.* Supramolecular control of the magnetic anisotropy in two-dimensional high-spin Fe arrays at a metal interface. *Nature Mater.* **8,** 189–193 (2009).
6. Brede, J. *et al.* Spin- and energy-dependent tunneling through a single molecule with intramolecular spatial resolution. *Phys. Rev. Lett.* **105,** 047204 (2010).
7. Barraud, C. *et al.* Unravelling the role of the interface for spin injection into organic semiconductors. *Nature Phys.* **6,** 615–620 (2010).
8. Atodiresei, N. *et al.* Design of the local spin polarization at the organic–ferromagnetic interface. *Phys. Rev. Lett.* **105,** 066601 (2010).
9. Javaid, S. *et al.* Impact on interface spin polarization of molecular bonding to metallic surfaces. *Phys. Rev. Lett.* **105,** 077201 (2010).
10. Atodiresei, N., Caciuc, V., Lazić, P. & Blügel, S. Engineering the magnetic properties of hybrid organic–ferromagnetic interfaces by molecular chemical functionalization. *Phys. Rev. B* **84,** 172402 (2011).
11. Mugarza, A. *et al.* Spin coupling and relaxation inside molecule–metal contacts. *Nature Commun.* **2,** 490 (2011).
12. Franke, K. J., Schulze, G. & Pascual, J. I. Competition of superconducting phenomena and Kondo screening at the nanoscale. *Science* **332,** 940–944 (2011).
13. Joachim, C., Gimzewski, J. K. & Aviram, A. Electronics using hybrid-molecular and mono-molecular devices. *Nature* **408,** 541–548 (2000).
14. Sanvito, S. Molecular spintronics. *Chem. Soc. Rev.* **40,** 3336–3355 (2011).
15. Callsen, M., Caciuc, V., Kiselev, N., Atodiresei, N. & Blügel, S. Magnetic hardening induced by nonmagnetic organic molecules. *Phys. Rev. Lett.* **111,** 106805 (2013).
16. Kawahara, S. L. *et al.* Large magnetoresistance through a single molecule due to a spin-split hybridized orbital. *Nano Lett.* **12,** 4558–4563 (2012).
17. Schwöbel, J. *et al.* Real-space observation of spin-split molecular orbitals of adsorbed single-molecule magnets. *Nature Commun.* **3,** 953 (2012).
18. Khajetoorians, A. A., Wiebe, J., Chilian, B. & Wiesendanger, R. Realizing all-spin-based logic operations atom by atom. *Science* **332,** 1062–1064 (2011).
19. Gambardella, P. *et al.* Giant magnetic anisotropy of single cobalt atoms and nanoparticles. *Science* **300,** 1130–1133 (2003).
20. Heinrich, A. J., Gupta, J. A., Lutz, C. P. & Eigler, D. M. Single-atom spin-flip spectroscopy. *Science* **306,** 466–469 (2004).
21. Meier, F., Zhou, L., Wiebe, J. & Wiesendanger, R. Revealing magnetic interactions from single-atom magnetization curves. *Science* **320,** 82–86 (2008).
22. Loth, S., Baumann, S., Lutz, C. P., Eigler, D. M. & Heinrich, A. J. Bistability in atomic-scale antiferromagnets. *Science* **335,** 196–199 (2012).
23. Khajetoorians, A. A. *et al.* Current-driven spin dynamics of artificially constructed quantum magnets. *Science* **339,** 55–59 (2013).
24. Heinze, S. *et al.* Spontaneous atomic-scale magnetic skyrmion lattice in two dimensions. *Nature Phys.* **7,** 713–718 (2011).
25. Decker, R. *et al.* Atomic-scale magnetism of cobalt-intercalated graphene. *Phys. Rev. B* **87,** 041403 (2013).
26. Raman, K. V. *et al.* Interface-engineered templates for molecular spin memory devices. *Nature* **493,** 509–513 (2013).
27. Ouazi, S. *et al.* Magnetization reversal of individual Co nanoislands. *Phys. Rev. Lett.* **108,** 107206 (2012).
28. Menzel, M. *et al.* Information transfer by vector spin chirality in finite magnetic chains. *Phys. Rev. Lett.* **108,** 197204 (2012).
29. Kresse, G. & Hafner, J. *Ab initio* molecular dynamics for liquid metals. *Phys. Rev. B* **47,** 558–561 (1993).
30. Kresse, G. & Furthmüller, J. Efficient iterative schemes for *ab initio* total-energy calculations using a plane-wave basis set. *Phys. Rev. B* **54,** 11169–11186 (1996).

Acknowledgements

The authors acknowledge financial support from the Deutsche Forschungsgemeinschaft (SFB 668 and SPP 1538) and from the European Union (ERC Advanced Grant FURORE). Computations were performed under the auspices of the Kommision zur Vergabe von Supercomputing Ressourcen (computer JUROPA) and the Gauss Centre for Supercomputing (the high-performance computer JUQUEEN operated by the Jülich Supercomputing Centre at the Forschungszentrum Jülich). J.B. is grateful for insightful discussions with A. Kubetzka and K. von Bergmann and for help from R. Decker before this project.

Author contributions

J.B. and N.A. conceived the experiment. J.B. carried out the measurements and analysed the experimental data. M.B. supported the measurements. N.A., V.C. and A.A-Z. carried out and analysed the DFT calculations. J.B. and R.W. wrote the manuscript. All authors discussed the results and commented on the manuscript.

Additional information

Supplementary information is available in the online version of the paper. Reprints and permissions information is available online at www.nature.com/reprints. Correspondence and requests for materials should be addressed to J.B. and N.A.

Competing financial interests

The authors declare no competing financial interests.